



# Design of Diarylheptanoid Derivatives as Dual Inhibitors Against Class IIa Histone Deacetylase and $\beta$ -amyloid Aggregation

Liang-Chieh Chen<sup>1,2</sup>, Hui-Ju Tseng<sup>3</sup>, Chang-Yi Liu<sup>4</sup>, Yun-Yi Huang<sup>1</sup>, Cheng-Chung Yen<sup>1</sup>, Jing-Ru Weng<sup>5</sup>, Yeh-Lin Lu<sup>1,2</sup>, Wen-Chi Hou<sup>1</sup>, Tony E. Lin<sup>4</sup>, I-Horng Pan<sup>6</sup>, Kuo-Kuei Huang<sup>6</sup>, Wei-Jan Huang<sup>1,3,7,8\*</sup> and Kai-Cheng Hsu<sup>4\*</sup>

<sup>1</sup> Graduate Institute of Pharmacognosy, College of Pharmacy, Taipei Medical University, Taipei, Taiwan, <sup>2</sup> School of Pharmacy, College of Pharmacy, Taipei Medical University, Taipei, Taiwan, <sup>3</sup> Ph.D. Program in Biotechnology Research and Development, College of Pharmacy, Taipei Medical University, Taipei, Taiwan, <sup>4</sup> Graduate Institute of Cancer Biology and Drug Discovery, College of Medical Science and Technology, Taipei Medical University, Taipei, Taiwan, <sup>5</sup> Department of Marine Technology and Resources, College of Marine Sciences, National Sun Yat-sen University, Kaohsiung, Taiwan, <sup>6</sup> Herbal Medicinal Product Division, Industrial Technology Research Institute, Hsinchu, Taiwan, <sup>7</sup> Ph.D. Program for the Clinical Drug Discovery from Botanical Herbs, College of Pharmacy, Taipei Medical University, Taipei, Taiwan, <sup>8</sup> School of Pharmacy, National Defense Medical Center, Taipei, Taiwan

## OPEN ACCESS

### Edited by:

Agata Copani,  
Università degli Studi di Catania, Italy

### Reviewed by:

Giovanna Cenini,  
Universität Bonn, Germany  
Adriana Pietropaolo,  
Università degli Studi Magna Græcia  
di Catanzaro, Italy

### \*Correspondence:

Wei-Jan Huang  
wjhuang@tmu.edu.tw  
Kai-Cheng Hsu  
piki@tmu.edu.tw

### Specialty section:

This article was submitted to  
Experimental Pharmacology  
and Drug Discovery,  
a section of the journal  
Frontiers in Pharmacology

Received: 19 March 2018

Accepted: 12 June 2018

Published: 03 July 2018

### Citation:

Chen L-C, Tseng H-J, Liu C-Y,  
Huang Y-Y, Yen C-C, Weng J-R,  
Lu Y-L, Hou W-C, Lin TE, Pan I-H,  
Huang K-K, Huang W-J and Hsu K-C  
(2018) Design of Diarylheptanoid  
Derivatives as Dual Inhibitors Against  
Class IIa Histone Deacetylase  
and  $\beta$ -amyloid Aggregation.  
*Front. Pharmacol.* 9:708.  
doi: 10.3389/fphar.2018.00708

Alzheimer's disease (AD) is a progressive neurodegenerative disorder with multiple etiologies. Beta-amyloid (A $\beta$ ) self-aggregation and overexpression of class IIa histone deacetylases (HDACs) are strongly implicated with AD pathogenesis. In this study, a series of novel diarylheptanoid derivatives were designed, synthesized and evaluated for use as dual A $\beta$  self-aggregation and class IIa HDAC inhibitors. Among these compounds, **4j**, **5c**, and **5e** displayed effective inhibitions for A $\beta$  self-aggregation, HDAC5 activity and HDAC7 activity with IC<sub>50</sub> values of <10  $\mu$ M. The compounds contain three common features: (1) a catechol or pyrogallol moiety, (2) a carbonyl linker and (3) an aromatic ring that can function as an HDAC cap and create hydrophobic interactions with A $\beta$ <sub>1–42</sub>. Furthermore, compounds **4j**, **5c**, and **5e** showed no significant cytotoxicity to human neuroblastoma SH-SY5Y cells and also exhibited neuroprotective effect against H<sub>2</sub>O<sub>2</sub>-induced toxicity. Overall, these promising *in vitro* data highlighted compounds **4j**, **5c**, and **5e** as lead compounds that are worthy for further investigation.

**Keywords:** Alzheimer's disease, A $\beta$  aggregation, histone deacetylase, isoform-selective inhibitors, dual inhibitors

## INTRODUCTION

Alzheimer's disease (AD) is a progressive neurodegenerative disorder that occurs more frequently in the elderly and is one of the most common causes of dementia. The pathology of AD is multifactorial and not yet fully understood. Current hypotheses include: extracellular deposition of beta-amyloid (A $\beta$ ), formation of intracellular neurofibrillary tangles by hyperphosphorylated tau protein, acetylcholine deficiency, glutamate excitotoxicity, neuroinflammation and widespread neuronal loss (Ahn et al., 2017; Hung and Fu, 2017). Due to the multiple pathogenic mechanisms in AD, a single target drug may not ameliorate the disease. Therefore, multi-target drugs may be a more prudent choice for developing AD therapeutics (Leon et al., 2013).

The amyloid hypothesis is generally believed to be responsible for the formation of senile plaques in the brain of patients with AD (Hardy and Selkoe, 2002; Bu et al., 2016). Beta-amyloid plaques are formed when amyloid precursor protein (APP) is cleaved by  $\beta$ - and  $\gamma$ -secretase to produce  $A\beta$  monomers with 38 to 42 amino acids (Hardy and Selkoe, 2002; Kuperstein et al., 2010; Bu et al., 2016). Among them,  $A\beta_{1-40}$  is the most abundant. However,  $A\beta_{1-42}$  has lower solubility than  $A\beta_{1-40}$  and thus, is more susceptible to self-aggregation, which can lead to different degrees of neurotoxicity (Gilbert, 2013; Bu et al., 2016). Studies have shown that increasing the  $A\beta_{1-42}$ :  $A\beta_{1-40}$  ratio can stabilize toxic  $A\beta$  oligomers (Kuperstein et al., 2010). Therefore, the inhibition of  $A\beta$  self-aggregation is a potential strategy for prevention or treatment of AD.

The class IIa isozymes HDAC5 and 7 are closely associated with AD (Koseki et al., 2012; Anderson et al., 2015). Additionally, class IIa HDACs are highly expressed in the brain regions associated with learning and memory and distributed in specific tissues, such as the brain, lung or heart (Bolden et al., 2006; Volmar and Wahlestedt, 2015). HDAC5 is increased in the frontal cortex of AD patients compared to control patients (Anderson et al., 2015). Overexpression of HDAC7 decreased  $\beta$ -catenin activity (Margariti et al., 2010). Downregulation of Wnt/ $\beta$ -catenin signaling has been implicated AD progression (Fischer et al., 2010; Vallee and Lecarpentier, 2016). Furthermore, *in vitro* studies using trichostatin A (TSA), a histone deacetylase (HDAC) inhibitor, resulted in a significant up-regulation of  $A\beta$  degrading enzyme neprilysin (NEP) expression in SH-SY5Y cells (Kerridge et al., 2014). These studies suggest that the inhibition of class IIa HDAC activity is a promising strategy for the treatment of AD.

Due to the complex etiology of AD, developing a multi-target drug may present significant clinical efficacy (Leon et al., 2013). This strategy can avoid disadvantages seen in single target drugs that only offer a palliative treatment (Leon et al., 2013). In recent years, many studies have focused on combining at least two pharmacophoric moieties into one molecule to increase efficacy of drugs (De Simone et al., 2017; Taguchi et al., 2017; Xu et al., 2018). Flavonoids (e.g., morin, myricetin, and quercetin) are polyphenolic compounds that contain a catechol or pyrogallol scaffold and have shown inhibition of  $A\beta$  self-aggregation (Figure 1, blue section) (Bu et al., 2016). The FDA approved HDAC inhibitor suberoylanilide hydroxamic acid (SAHA) contains an aliphatic-chain linker and a hydrophobic benzene cap (Figure 1, red section) (Miller et al., 2003). Furthermore, another compound with neuroprotective effect is yakuchinone B, which contains an  $\alpha$ ,  $\beta$ -unsaturated carbonyl of yakuchinone B extends a  $\pi$ -electron system in conjugation with the phenyl ring (Figure 1, green section) (Jang et al., 2009; Lee et al., 2014). Thus, these structures, which are potential therapies for AD, can be exploited to create a dual  $A\beta$  and HDAC inhibitor.

In this study, we designed and synthesized a series of diarylheptanoid derivatives as dual  $A\beta$  self-aggregation and class IIa HDAC inhibitors. The inhibitory potency of the compounds was evaluated for  $A\beta_{1-42}$  self-aggregation and HDAC activity. Then, the compounds were virtually docked to

analyze their structure-activity relationship (SAR). Furthermore, *in vitro* cytotoxicity and neuroprotective effects of the synthesized compounds were investigated. The compounds in this study may have the potential for use in AD treatments.

## MATERIALS AND METHODS

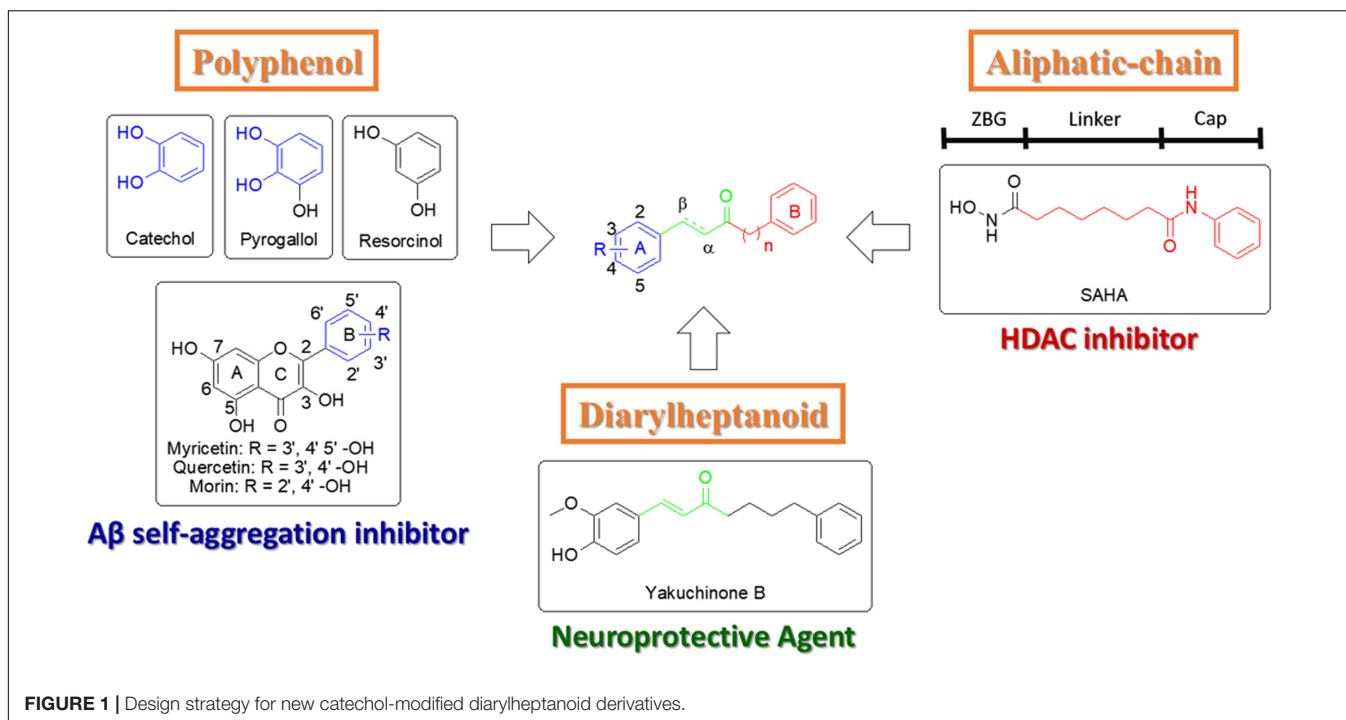
### Materials

The NMR spectra ( $^1\text{H}$  and  $^{13}\text{C}$  NMR) were obtained with a Bruker Fourier 300 and AVIII 500 using standard pulse programs, and chemical shifts are cited in parts per million (ppm,  $\delta$ ) downfield from TMS as an internal standard. NMR data were processed using Bruker TOPSPIN software. The MS data was measured on Finnigan Mat TSQ-7000 mass spectrometer (HRESIMS) (Thermo, Ringoes, NJ, United States). The HPLC was performed on a C18 column (150 mm  $\times$  4.6 mm, Ascentis) by an L-2130 pump (Hitachi, Ibaraki, Japan) and a UV/vis L-2420 detector (Hitachi, Ibaraki, Japan). The column chromatography was performed on silica gel (70–230 mesh, Merck, Darmstadt, Germany). All TLC analyses were performed on silica gel plates (KG60-F254, Merck). The microplate spectrophotometer was used for fluorometric analysis by Victor 2X (Perkin Elmer, Fremont, CA, United States) and absorbance analysis by Sunrise microplate reader (TECAN, Männedorf, Switzerland) or Synergy HT (Bio-Tek, Winooski, VT, United States). The microplate incubator shaker was used for ThT assay by BioShake iQ ThermoMixer (Quantifoil Instruments GmbH, Jena, Germany). Unless otherwise mentioned, reagents and materials were used without further purification and purchased from ACROS (Geel, Belgium). 3, 4-Dihydroxybenzaldehyde and 2, 3-dihydroxybenzaldehyde was purchased from Alfa Aesar (Haverhill, MA, United States). 3-Fluoro-4-hydroxybenzaldehyde, 3-chloro-4-hydroxybenzaldehyde, 3-bromo-4-hydroxybenzaldehyde and 1-(triphenylphosphoranylidene)propan-2-one was purchased from AK Scientific (Union City, CA, United States). Tributyl(1-ethoxyvinyl)tin was purchased from Combi-Blocks (San Diego, CA, United States). 10% Pd-C was purchased from Sigma-Aldrich (Saint Louis, MO, United States). Dry dichloromethane (DCM) was distilled from  $\text{CaH}_2$  under nitrogen atmosphere. All reactions were conducted under an atmosphere of dry  $\text{N}_2$ .

### Chemistry

#### General Procedure for the Synthesis of Compounds 2 and 11 by Wittig Olefination

To a solution of 1-(triphenylphosphoranylidene)propan-2-one (1.2 equiv) in dry DCM was added compound 1 or 10 (1 equiv) dropwise by syringe, respectively. The resulting mixture was heated to reflux and stirred for 12 h. The reaction mixture was concentrated in vacuo, diluted with EtOAc (100 mL) and washed with distilled  $\text{H}_2\text{O}$  (3  $\times$  50 mL). The organic layer was dried over  $\text{Na}_2\text{SO}_4$ , filtered and concentrated in vacuo. The residue was purified by silica gel chromatography (EtOAc: *n*-hexane = 1:9) to give  $\alpha$ ,  $\beta$ -unsaturated ketones 2 (5.1 g, 79%) and 11 (213 mg, 87%).



### General Procedure for the Synthesis of Compounds 3, 5a–i, 6d, and 8a–d by Hydrogenation

A catalytic amount of 10% Pd-C was added to a solution of unsaturated compounds in EtOH and the mixture was stirred at RT under H<sub>2</sub> atmosphere for 5 h. The reaction mixture was filtered with celite and the filtrate was concentrated in vacuo. The residue was purified by silica gel chromatography (EtOAc: *n*-hexane = 1:11) to give  $\alpha$ ,  $\beta$ -saturated ketones **3** (5.1 g, 99%), **5a** (35 mg, 97%), **5b** (52 mg, 95%), **5c** (51 mg, 99%), **5d** (70 mg, 77%), **5e** (79 mg, 78%), **5f** (55 mg, 61%), **5g** (37 mg, 37%), **5h** (39 mg, 39%), **5i** (96 mg, 99%), **6d** (187 mg, 95%), **8a** (30 mg, 60%), **8b** (21 mg, 52%), **8c** (33 mg, 66%) and **8d** (27 mg, 67%).

### General Procedure for the Synthesis of Compounds 4a–k and 7a–d by Aldol Condensation

To a solution of compound **3** (1.5 equiv) in THF was added pyrrolidine (1.5 equiv), acetic acid (1.5 equiv) and benzaldehyde (1 equiv). The mixture was heated to reflux for 6 h. The reaction mixture was diluted with EtOAc (100 mL) and washed with distilled H<sub>2</sub>O (3  $\times$  50 mL). The organic layer was dried over Na<sub>2</sub>SO<sub>4</sub>, filtered and concentrated in vacuo. The residue was purified by silica gel chromatography (EtOAc: *n*-hexane = 1:15) to give diarylheptanoid **4a** (226 mg, 73%), **4b** (156 mg, 89%), **4c** (94 mg, 50%), **4d** (54 mg, 34%), **4e** (225 mg, 67%), **4f** (125 mg, 74%), **4g** (61 mg, 34%), **4h** (110 mg, 54%), **4i** (109 mg, 59%), **4j** (85 mg, 48%), **4k** (95 mg, 62%), **7a** (145 mg, 73%), **7b** (51 mg, 29%), **7c** (130 mg, 72%), and **7d** (104 mg, 72%).

### Synthesis of Compound 6b by Stille Coupling Reaction

To a mixture of compound **9** (1 equiv) and PdCl<sub>2</sub>(PPh<sub>3</sub>)<sub>2</sub> (0.1 equiv) in toluene (5 mL) was added tributyl(1-ethoxyvinyl)tin

(1.1 equiv). The resulting solution was heated to 80°C and stirred for 20 h. After cooling to RT, the reaction mixture was acidified with 1 M HCl (aq) and stirred for 3 h. The mixture was diluted with EtOAc (30 mL) and washed with distilled H<sub>2</sub>O (3  $\times$  30 mL). The organic layer was dried over Na<sub>2</sub>SO<sub>4</sub>, filtered and concentrated in vacuo. The residue was purified by silica gel chromatography (EtOAc: *n*-hexane = 1:9) to give compound **6b** (421 mg, 79%). The experimental details and physical data of all synthetic compounds can be found in the Supplementary Materials.

## Pharmacological Assay

### Inhibition of A $\beta$ <sub>1–42</sub> Self-Aggregation

Inhibition of A $\beta$ <sub>1–42</sub> self-aggregation was measured by thioflavin-T (ThT) fluorescence assay (Hudson et al., 2009). A $\beta$ <sub>1–42</sub> peptides were purchased from Kelowna International Scientific Inc. To avoid A $\beta$ <sub>1–42</sub> self-aggregation before the start of the experiment, A $\beta$ <sub>1–42</sub> peptides were dissolved in hexafluoroisopropanol (HFIP) to a concentration of 1 mM. The clear solution containing the dissolved peptide was then aliquoted in micro centrifuge tube. The solution was evaporated under vacuum to remove HFIP to give monomeric A $\beta$ <sub>1–42</sub>. The monomeric A $\beta$ <sub>1–42</sub> was dissolved in NaOH<sub>(aq)</sub> (60 mM) to give a stock solution (1 mM). The A $\beta$ <sub>1–42</sub> stock solution was diluted with 50 mM phosphate buffer (containing 0.15 M NaCl, pH 7.4) before use. Fresh ThT stock solution was prepared by dissolving ThT (Sigma, T3516) in phosphate buffer and filtrated through 0.45  $\mu$ m Nylon syringe filter. The ThT stock solution and 400 mM ethylenediaminetetraacetic acid (EDTA) were diluted into the phosphate buffer to generate the working solution as background. A mixture of working

solution (ThT final concentration: 10  $\mu\text{M}$ ),  $\text{A}\beta_{1-42}$  stock solution ( $\text{A}\beta_{1-42}$  final concentration: 10  $\mu\text{M}$ ) and the tested compounds were incubated on BioShake iQ ThermoMixer (37°C, 700 rpm) for 24 h. Fluorescence was measured by Victor 2X microplate spectrophotometer (excitation  $\lambda = 440$  nm, emission  $\lambda = 486$  nm), and adapted for 96-well microtiter plates. The fluorescence intensities were recorded and the percent inhibition due to the presence of the inhibitors were calculated by the following formula:  $(1 - \text{IF}_i/\text{IF}_c) \times 100\%$  where  $\text{IF}_i$  and  $\text{IF}_c$  were the fluorescence intensities obtained for  $\text{A}\beta_{1-42}$  in the presence and in the absence of inhibitors after subtracting the background, respectively. The  $\text{IC}_{50}$  values were calculated by the linear regression model of the data. All experiments were performed in triplicate.

### Preparation of HDAC4

Preparation of HDAC4 was performed as previously described (Huang et al., 2012). Genes encoding HDAC4 (residues 648–1057) flanked with NdeI and EcoRI sites at the 5'- and 3'-ends, were synthesized by GenScript Corporation (Piscataway, NJ, United States) and subcloned into expression vectors pET-28a(b) and pET-24b(b). Proteins were expressed in BL21(DE3) cells by overnight induction with IPTG (1 mM) at 20–25°C and purified from cleared cell lysates by sequential chromatography on Ni-Sepharose 6 fast flow, Mono Q 5/50 GL, and Superdex 75 10/300 GL columns (GE Healthcare). Protein concentrations were quantified with Bradford Reagent (Bio-Rad).

### Inhibition of HDACs

Inhibition of HDACs were measured by the HDAC fluorometric activity assays (Wegener et al., 2003). Enzyme, inhibitors and substrate were diluted with HDAC buffer (15 mM Tris-HCl pH 8.1, 0.25 mM EDTA, 250 mM NaCl, 10% v/v glycerol). Briefly, 10  $\mu\text{L}$  diluted HDAC, i.e., HeLa nuclear extract (Enzo), HDAC6 (BPS), HDAC4, HDAC5 (BPS), HDAC7 (BPS) and HDAC9 (BPS), as well as 50  $\mu\text{L}$  of testing compounds at different concentrations were added to each well of a 96-well microtiter plate and pre-incubated at 30°C for 5 min. The enzymatic reaction was started by addition 40  $\mu\text{L}$  substrate, including Boc-Lys(Ac)-AMC (Bachem) 10  $\mu\text{M}$  for HeLa nuclear extract and HDAC6, and Boc-Lys(TFA)-AMC (Bachem) 10  $\mu\text{M}$  for HDAC4, fluorogenic HDAC class IIa substrate, Catalog #: 50040 (BPS Bioscience, San Diego, CA, United States) 10  $\mu\text{M}$  for HDAC5, HDAC7 and HDAC9 into the HDAC buffer. After incubation at 37°C for 30 min, the reaction was stopped by adding 100  $\mu\text{L}$  trypsin solution (10 mg/mL trypsin in 50 mM Tris-HCl pH 8, 100 mM NaCl, 2 mM SAHA). After incubation at 37°C for another 20 min, fluorescence was measured (excitation  $\lambda = 355$  nm, emission  $\lambda = 460$  nm) with VICTOR X2 microplate spectrophotometer. The fluorescence in wells without test compounds (0.1% DMSO, negative control) was set as 100% enzymatic activity and the fluorescence in wells with enzyme eliminated was set as 0% enzymatic activity. The fluorescence ratio of test compounds to negative control was defined as percentage of remaining enzyme activity. The  $\text{IC}_{50}$  values were calculated by linear regression of the data. All experiments were performed in triplicate.

### Molecular Modeling Analysis

The computational analysis was executed using Discovery Studio (DS) (BIOVIA et al., 2016). The CDOCKER program in DS was used for molecular docking of  $\text{A}\beta_{1-42}$  and HDAC7. Structures for  $\text{A}\beta_{1-42}$  (PDB ID: 1Z0Q) and HDAC7 (PDB ID: 3ZNS) were obtained from Protein Data Bank (PDB). The structures were then prepared by the automatic ligand preparation function in DS Macromolecules Tools for protonation, removal of water molecules and mismatched residues fixing. The protonated state was set to 7.4 pH. The  $\text{A}\beta_{1-42}$  binding site was detected automatically with a 10 Å radius sphere by DS. The HDAC7 binding site was defined by the co-crystallized ligand within a 10 Å radius sphere. The compounds were prepared by the ligand preparation function in DS Small Molecules Tools for protonation and fixing bad valence. The compounds were then docked to the binding sites by the Docking Optimization function of CDOCKER using the following parameters: random conformations of each ligand were set to 30, refined orientations for each conformation was set to 30 and a value of maximum bad orientations was set to 1600. The simulated annealing for each orientation was set for heating to 700 K over 2,000 steps followed by cooling to 300 K over 5,000 steps. The CHARMM forcefield and Momany-Rone ligand partial charge method were employed for the scoring function to generate the docking score called -CDOCKER interaction energy. In total, the program generated 10 top-ranked poses for each compound and generated an interaction profile of all poses using the DS interaction analysis function. Final binding poses of each compound in  $\text{A}\beta_{1-42}$  and HDAC7 were selected according to their -CDOCKER interaction energy. All binding poses have a -CDOCKER interaction energy score of at least 30 for HDAC7 and at least 20 for  $\text{A}\beta_{1-42}$ . Total energy was generated for each pose using the CHARMM forcefield in DS with the following parameters: solvent model set to none, non-bond list radius set to 14.0 Å and electrostatics set to automatic. We identified a maximum common substructure (MCSS) of all compounds. This was used to create a root-mean-square deviation (RMSD) analysis. The absorption, distribution, metabolism, excretion and toxicity (ADMET) was calculated using the ADMET component in DS. Each category is separated into different levels: blood brain barrier (BBB) penetration levels 0 (very high) to 4 (undefined), human intestinal absorption levels 1 (very low solubility) to 5 (very soluble) and absorption level 0 (good solubility) to 3 (very low solubility). The ADMET component used default parameters.

### Cell Culture

SH-SY5Y cells were kindly provided by Professor Zhi-Hong Wen (National Sun Yat-sen University) and cultured in DMEM/F12 (Gibco, Grand Island, NY, United States) supplemented with 10% heat-inactivated fetal bovine serum and penicillin (100 U/ml)/streptomycin (100  $\mu\text{g}/\text{ml}$ ) (Invitrogen, Carlsbad, CA, United States) at 37°C in an atmosphere of 5%  $\text{CO}_2$ .

### Cytotoxicity Effect on SH-SY5Y Cells

Cell viability was assessed using the alamar blue (7-hydroxy-10-oxidophenoxazin-10-ium-3-one) cell viability assay in 6 replicates as described previously (Feng et al., 2016). Briefly,

$5 \times 10^3$  cells/well were seeded in 96-well flat-bottomed plates; 24 h later, cells were treated with compounds or DMSO as control. After 24 h of incubation, the medium was removed, 100  $\mu$ L medium containing 10  $\mu$ L of alamar blue was added, and cells were incubated in the 5% CO<sub>2</sub> incubator at 37°C for 4 h. Absorbance at 570 nm was determined by Synergy HT microplate reader. The results were averaged over three different independent experiments. The cell viability was also evaluated by trypan blue exclusion test.

### Neuroprotection Against H<sub>2</sub>O<sub>2</sub>-Induced Neurotoxicity on SH-SY5Y Cells

H<sub>2</sub>O<sub>2</sub>-induced neurotoxicity on SH-SY5Y cells was used to evaluate the neuroprotective effect (Rafatian et al., 2012; Omar et al., 2017). Briefly, a density of  $2 \times 10^4$  SH-SY5Y cells were seeded per well in 96-well plates. After 24 h of incubation, the medium was replaced with serum free medium containing H<sub>2</sub>O<sub>2</sub> at a concentration of 500  $\mu$ M and treated with different concentrations of compounds (40, 20, and 10  $\mu$ M). SH-SY5Y cells were also cultured without any treatment as control group and results were indicated by percentage of control. After 3 h, cell viability was performed by MTT assay. The cells were treated with MTT (5 mg/ml in PBS) for 4 h at 37°C. The formazan crystals were generated by viable mitochondrial succinate dehydrogenase from MTT. The supernatant was then aspirated off and the formazan crystals were dissolved with DMSO. Absorbance at 570 nm was determined by Tecan Sunrise microplate reader. The trypan blue exclusion test was also used to evaluate the neuroprotection.

## RESULTS AND DISCUSSIONS

### Chemistry

We designed dual inhibitors using the diarylheptanoid scaffold as the core structure, due to its linear structure and neuroprotective capabilities seen in previous studies (Jang et al., 2009) (Scheme 1). First, we synthesized various compounds with different substituted groups on the A ring. Polyphenols were used to achieve A $\beta$ <sub>1–42</sub> self-aggregation and HDAC IIa inhibition (Bu et al., 2016). Therefore, we added a number of hydroxy groups and electron-donating or electron-withdrawing groups on the A ring. Compounds 4a–4k and 5a–5i were synthesized as described in Scheme 1. Wittig olefination of compound 1 with 1-(triphenylphosphoranylidene)propan-2-one generated compound 2. Compound 2 treated with the catalytic amount of 10% Pd-C to afford compound 3. Aldol condensation of compound 3 using various substituted benzaldehyde gave desired diarylheptanoids 4a–4k. Repeated hydrogenation of compounds 4a–4k produced compounds 5a–5i, respectively.

Next, to investigate the effects of carbon linker chain on the A $\beta$ <sub>1–42</sub> self-aggregation and HADC inhibition, we carried out the synthesis of compounds 7a–7d and 8a–8d. These compounds contain various chain lengths of the carbon linker as described in Scheme 2. Stille coupling of compound 9 with tributyl(1-ethoxyvinyl)tin in the presence of PdCl<sub>2</sub>(PPh<sub>3</sub>)<sub>2</sub> afforded compound 6b. Wittig olefination of compound 10

yielded compound 11. Hydrogenation of compound 11 gave compound 6d. Aldol condensation of varied methyl ketones 6a–6d with 3,4-dihydroxybenzaldehyde produced corresponding  $\alpha,\beta$ -unsaturated ketones 7a–7d. Finally, hydrogenation of compounds 7a–7d yielded compounds 8a–8d, respectively. The <sup>1</sup>H and <sup>13</sup>C NMR spectra can be found in the Supplementary Figures S1–S61. All compounds had an estimated purity of at least 97% as determined by HPLC analysis (Supplementary Figures S62–S89).

## Biological Assays and Molecular Docking Analysis

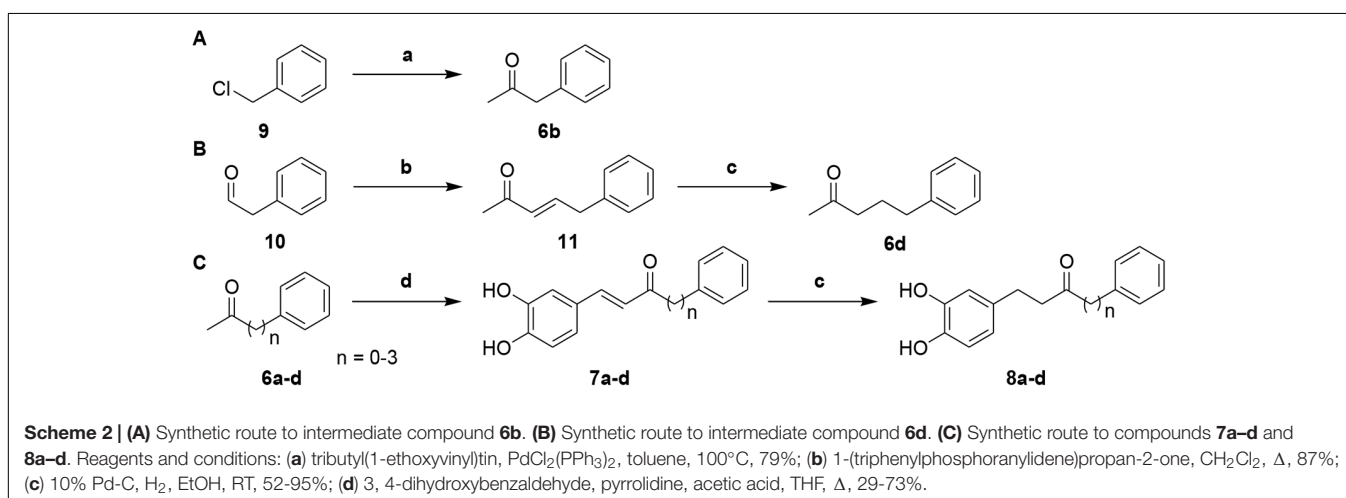
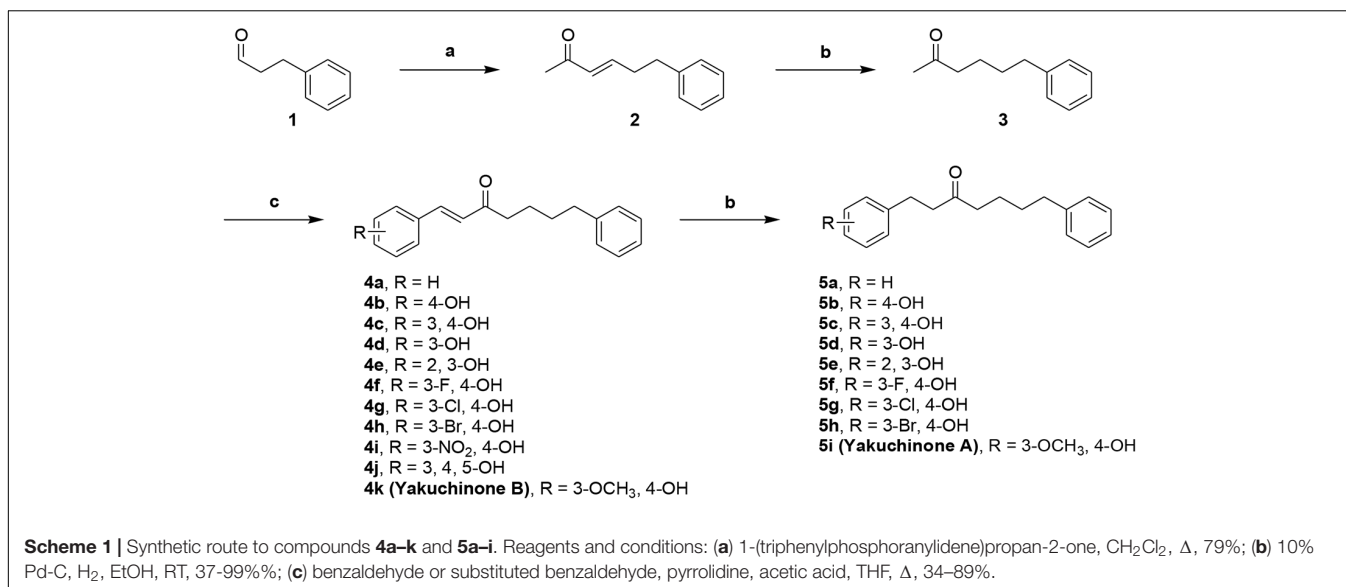
### Inhibition of A $\beta$ <sub>1–42</sub> Self-Aggregation

The synthesized compounds were evaluated for their inhibitory potency of A $\beta$ <sub>1–42</sub> self-aggregation, using a ThT fluorescence assay (Hudson et al., 2009). First, the compounds were screened at a single concentration of 10  $\mu$ M. Then, the compounds with an inhibition ratio of  $\geq 50\%$  were selected to determine their IC<sub>50</sub> values. The inhibition ratio and IC<sub>50</sub> values of the compounds were listed in Table 1. In general, the compounds were divided into two groups according to their chemical structures. Compounds in group one retains the diarylheptanoid scaffold and the substituents on the A ring synthesized from Scheme 1 (compounds 4a–k and 5a–i). Among this group, compounds 4c, 4e, 4j, 5c, and 5e contain either a catechol or pyrogallol moiety. They exhibited potent inhibitions for A $\beta$ <sub>1–42</sub> self-aggregation with IC<sub>50</sub> values of 6.1, 3.4, 3.6, 5.8, and 6.0  $\mu$ M, respectively. Additionally, these five compounds showed better inhibitory activity than the reference compounds morin and SAHA. Interestingly, these five compounds have catechol (compounds 4c, 4e, 5c, and 5e) or pyrogallol (compound 4j) groups on the A ring. These results were in line with the inhibition of A $\beta$ <sub>1–42</sub> self-aggregation by polyphenol. However, when we modified the 3-position of the A ring with an electron-donating or electron-withdrawing group (e.g., fluoro, nitro, etc.), we did not observe a significant increase in inhibitory activity. These results suggested that a catechol or pyrogallol moiety connected with  $\alpha,\beta$ -unsaturated carbonyl group plays a key role for the inhibition of A $\beta$ <sub>1–42</sub> self-aggregation.

The compounds of group two were synthesized to assess the effect of the linker length. Thus, compounds 7a–d and 8a–d retain the catechol and  $\alpha,\beta$ -unsaturated carbonyl moieties, but possess shorter linkers. The most potent inhibitor was compound 7b, which has an IC<sub>50</sub> value of 2.1  $\mu$ M. Furthermore, we found that  $\alpha,\beta$ -unsaturated compounds significantly increased activity when compared to saturated compounds. Moreover, the compounds with the shorter linkers showed increased inhibitory activity compared to those with the longer linkers, such as compound 4c. These experimental results indicated that compounds 4c, 4e, 4j, 5c, 5e, 7a–d, and 8a–d can reduce A $\beta$ <sub>1–42</sub> self-aggregation.

### Active Compounds Have Conserved Interactions With A $\beta$ <sub>1–42</sub>

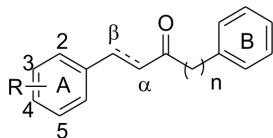
To investigate the SAR of the designed compounds, we performed molecular docking and interaction analysis using DS (BIOVIA et al., 2016). The synthesized compounds were



docked into A $\beta$ <sub>1–42</sub> (PDB ID: 1Z0Q) and contained a –CDOKER energy score ranging from 24 to 31. The total energy of protein-compound complexes can be found in Supplementary Table S1. In general, the A $\beta$ <sub>1–42</sub> active compounds have a lower total energy range. This indicates that the active compounds are more stable when bound to A $\beta$ <sub>1–42</sub>. The active compounds of group one (compounds **4c**, **4e**, **4j**, **5c**, and **5e**) produce similar interactions with the A $\beta$ <sub>1–42</sub> helix (**Figure 2A**). Compounds **4c** and **5c** contain a 3,4-dihydroxy group on the A ring, while compound **4j** contain a 3,4,5-trihydroxy group. The hydroxy groups on the A-ring 3 and 4 positions serve as hydrogen donors that form hydrogen bonds with residue D23. Simultaneously, the carbonyl group serve as a hydrogen acceptor and a hydrogen bond is formed with residue Q15. This type of binding conformation also produces favorable van der Waals (VDW) interactions between residues E11, H14, V18, F19 and E22 (**Figure 2B**). Similarly, compounds **4e** and **5e** contain a 2,3-dihydroxy group that can form hydrogen bonds with residue

D23. The carbonyl group form a hydrogen bond with residue Q15. In addition, the B ring position is closer to residues V18 and H14. This forms the  $\pi$ -alkyl interaction between residue V18 and compound **4e**, and VDW interactions with E11, H14, F19, and E22 (**Figure 2C**). Meanwhile, the inactive compound **4a** (IC<sub>50</sub> > 10  $\mu$ M) does not contain hydroxy groups on the A ring and does not form interactions with D23 (**Figure 2D**). These results suggest hydrogen donors are necessary to produce two hydrogen bonds with residue D23. In summary, we identified common interactions between the active compounds. In particular, two hydrogen bonds with residue D23, and one hydrogen bonds with Q15 (**Figure 2E**).

To study the effect of the linker length on activity, we compared the docking poses of compound **4c** with the active compounds (compounds **7a–d**) of group two (**Figure 3A**). Like compound **4c**, compounds **7a–d** displayed similar polar contacts to residues Q15 and D23 (**Figure 2E**). The shorter chain length allows the B ring of group two compounds to generate

**TABLE 1** | Inhibitions of compounds **4a–k**, **5a–i**, **7a–d**, **8a–d** and reference compounds against A $\beta$ <sub>1–42</sub> self-aggregation.

Compound	Substitution (R)	Chain length (n)	$\alpha$ , $\beta$ -saturation	Beta-Amyloid Aggregation	
				Inhibition (%) <sup>a,b</sup>	IC <sub>50</sub> ( $\mu$ M) <sup>b</sup>
<b>4a</b>	H	4	Unsaturated	11.9 $\pm$ 1.0%	>10
<b>4b</b>	4-OH	4	Unsaturated	28.7 $\pm$ 6.3%	>10
<b>4c</b>	3, 4-OH	4	Unsaturated	76.2 $\pm$ 2.7	6.1 $\pm$ 1.3
<b>4d</b>	3-OH	4	Unsaturated	0.7 $\pm$ 1.5	>10
<b>4e</b>	2, 3-OH	4	Unsaturated	91.7 $\pm$ 2.5	3.4 $\pm$ 0.6
<b>4f</b>	3-F, 4-OH	4	Unsaturated	34.9 $\pm$ 9.2	>10
<b>4g</b>	3-Cl, 4-OH	4	Unsaturated	27.8 $\pm$ 7.1	>10
<b>4h</b>	3-Br, 4-OH	4	Unsaturated	28.1 $\pm$ 2.1	>10
<b>4i</b>	3-NO <sub>2</sub> , 4-OH	4	Unsaturated	49.0 $\pm$ 2.9	>10
<b>4j</b>	3, 4, 5-OH	4	Unsaturated	78.7 $\pm$ 6.2	3.6 $\pm$ 1.0
<b>4k</b>	3-OCH <sub>3</sub> , 4-OH	4	Unsaturated	23.1 $\pm$ 6.4	>10
<b>5a</b>	H	4	Saturated	14.0 $\pm$ 3.0	>10
<b>5b</b>	4-OH	4	Saturated	30.4 $\pm$ 1.0	>10
<b>5c</b>	3, 4-OH	4	Saturated	67.8 $\pm$ 3.4	5.8 $\pm$ 0.2
<b>5d</b>	3-OH	4	Saturated	-22.1 $\pm$ 2.0	>10
<b>5e</b>	2, 3-OH	4	Saturated	65.9 $\pm$ 0.2	6.0 $\pm$ 0.9
<b>5f</b>	3-F, 4-OH	4	Saturated	22.1 $\pm$ 11.1	>10
<b>5g</b>	3-Cl, 4-OH	4	Saturated	17.8 $\pm$ 2.8	>10
<b>5h</b>	3-Br, 4-OH	4	Saturated	1.0 $\pm$ 3.0	>10
<b>5i</b>	3-OCH <sub>3</sub> , 4-OH	4	Saturated	4.6 $\pm$ 11.7	>10
<b>7a</b>	3, 4-OH	0	Unsaturated	83.1 $\pm$ 1.9	2.3 $\pm$ 0.2
<b>7b</b>	3, 4-OH	1	Unsaturated	79.4 $\pm$ 2.6	2.1 $\pm$ 0.2
<b>7c</b>	3, 4-OH	2	Unsaturated	83.7 $\pm$ 0.8	3.4 $\pm$ 0.4
<b>7d</b>	3, 4-OH	3	Unsaturated	74.0 $\pm$ 9.5	3.1 $\pm$ 0.3
<b>8a</b>	3, 4-OH	0	Saturated	66.4 $\pm$ 1.0	8.6 $\pm$ 1.1
<b>8b</b>	3, 4-OH	1	Saturated	68.6 $\pm$ 4.1	8.1 $\pm$ 1.2
<b>8c</b>	3, 4-OH	2	Saturated	71.3 $\pm$ 3.8	8.0 $\pm$ 1.6
<b>8d</b>	3, 4-OH	3	Saturated	59.0 $\pm$ 5.8	8.5 $\pm$ 0.2
<b>Morin</b>	-	-	-	56.9 $\pm$ 5.9	8.8 $\pm$ 0.7
<b>SAHA</b>	-	-	-	-13.3 $\pm$ 1.8	>10

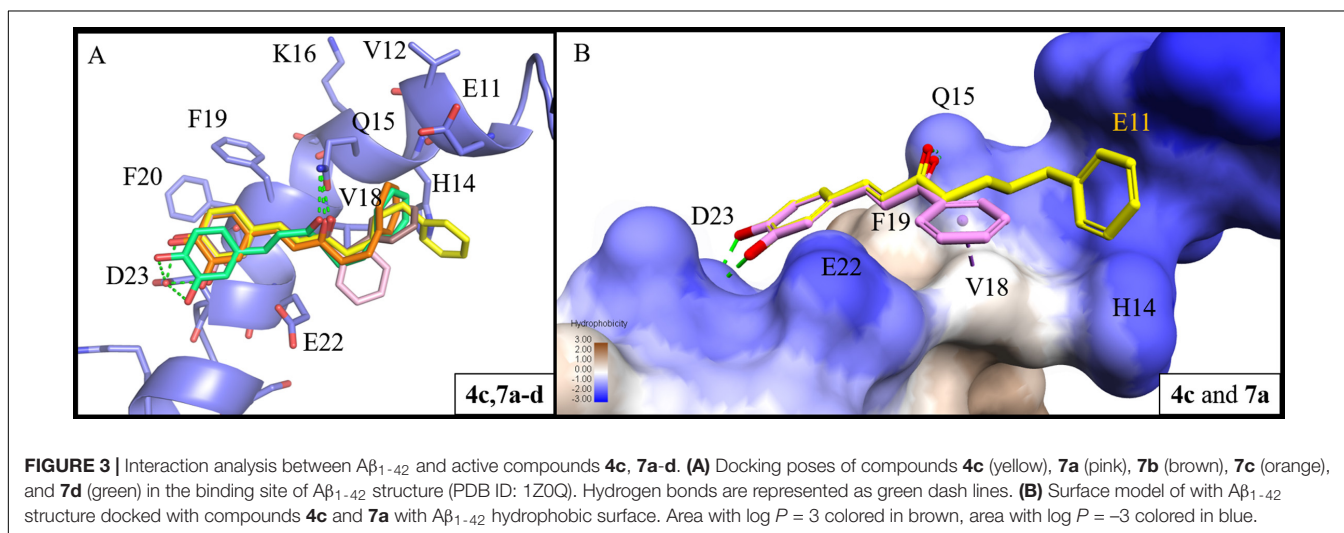
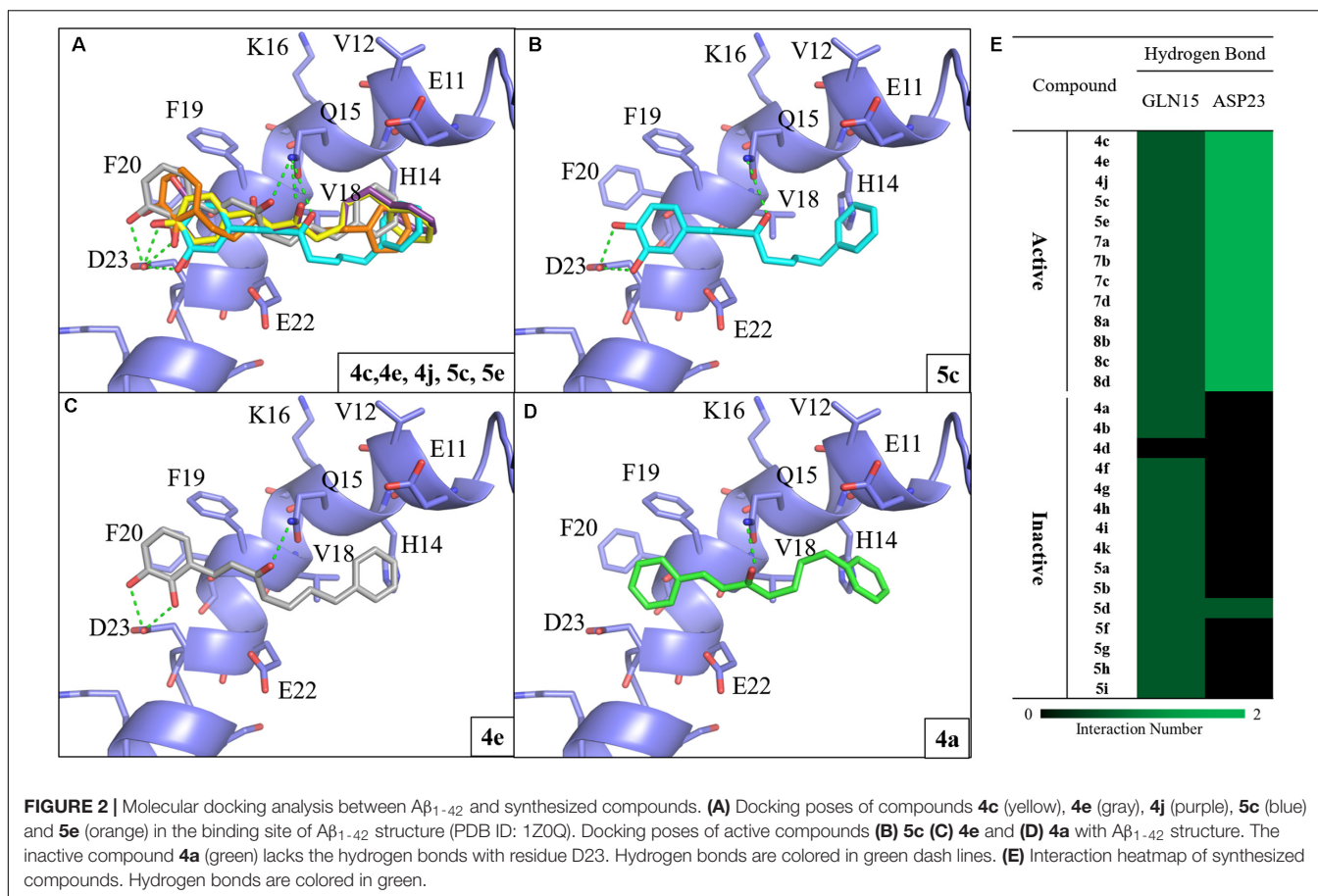
<sup>a</sup>The thioflavin-T (ThT) fluorescence assay was used to evaluate the inhibitory activity of compounds at a concentration of 10  $\mu$ M. <sup>b</sup>Each values are presented as the mean of three independent experiments.

$\pi$ -alkyl interaction with residue V18, which stabilize the binding of the compounds. Thus, compounds **7a–d** displayed better activity than compound **4c** (Figure 3B). The results showed that our compounds with the shorter carbon-linker had the best inhibitory results for A $\beta$ <sub>1–42</sub> self-aggregation.

We also identified the MCSS of all synthetic compounds (Supplementary Figure S90) to analyze the docking poses. The RMSD value between two binding poses was calculated according to the MCSS. The RMSD matrix was generated for all of the selected binding poses and revealed two clusters. Cluster 1 contains all active compounds and two inactive compounds, while the compounds in cluster 2 are inactive. RMSD values of intra binding poses in each cluster are <2 Å (Supplementary

Figure S91). The compounds in cluster 2 do not contain a catechol or pyrogallol moiety.

During the A $\beta$  self-aggregation process, the protein secondary structure element  $\alpha$ -helix undergoes a conformational change to  $\beta$ -sheet, which is linked to fibrillogenesis (Ding et al., 2003; Zhou et al., 2010). The synthesized compounds in our docking procedure form a hydrogen bond to residue Q15 as an anchor to the middle cavity of the A $\beta$ <sub>1–42</sub> structure. When comparing active and inactive compounds, hydrogen bonds with residue D23 appear to be the key for inhibitory activity. Therefore, the active compounds form interactions that disrupted A $\beta$ <sub>1–42</sub>  $\alpha$ -helix to  $\beta$ -sheet conversion to prevent A $\beta$  self-aggregation.



### Inhibition of HDACs

Next, we looked to test the synthesized compounds HDACs inhibitory activity with a HDAC fluorogenic assay and using SAHA as the control (Wegener et al., 2003). We determined their enzyme inhibiting effects against a panel of HDAC isoforms including class IIa (HDAC4, 5, 7, and 9), class IIb (HDAC6) and HaLa nuclear HDACs, which contain class I HDACs (Table 2).

Group one compounds (compounds **4a-k** and **5a-i**) contain a diarylheptanoid scaffold and various substituents on the A ring. We observed poor inhibitory activity on HeLa nuclear HDACs. However, group one compounds **4c**, **4e**, **4j**, **5c**, and **5e** displayed significant inhibitions of class IIa HDACs. Furthermore, the compounds showed an increased inhibition and selectivity toward HDAC class IIa compared to SAHA. Among these,

**TABLE 2** | IC<sub>50</sub> values (μM)<sup>a</sup> of compounds **4a–k**, **5a–i**, **7a–d**, **8a–d** and reference compound for HDAC inhibition.

Compound	HeLa Nuclear HDACs	Class IIa				Class IIb
		HDAC4	HDAC5	HDAC7	HDAC9	
<b>4a</b>	>40	>40	>40	>40	>40	>40
<b>4b</b>	>40	>40	>40	>40	>40	>40
<b>4c</b>	>40	30.5 ± 0.7	15.9 ± 1.5	8.4 ± 0.3	17.6 ± 0.3	18.3 ± 0.9
<b>4d</b>	>40	>40	>40	>40	>40	>40
<b>4e</b>	>40	38.8 ± 0.1	14.6 ± 0.2	8.6 ± 1.0	18.1 ± 0.4	29.4 ± 1.5
<b>4f</b>	>40	>40	>40	>40	>40	>40
<b>4g</b>	>40	>40	>40	>40	>40	>40
<b>4h</b>	>40	>40	>40	>40	>40	>40
<b>4i</b>	>40	>40	36.1 ± 3.7	32.7 ± 2.1	>40	>40
<b>4j</b>	>40	>40	7.1 ± 0.2	3.8 ± 0.4	15.4 ± 1.8	11.9 ± 0.2
<b>4k</b>	>40	>40	>40	>40	>40	>40
<b>5a</b>	>40	>40	>40	>40	>40	>40
<b>5b</b>	>40	>40	>40	>40	>40	>40
<b>5c</b>	>40	18.1 ± 0.8	3.8 ± 0.1	4.3 ± 0.5	5.3 ± 0.3	>40
<b>5d</b>	>40	>40	>40	>40	>40	>40
<b>5e</b>	>40	35.9 ± 0.1	4.8 ± 0.4	8.7 ± 0.7	9.3 ± 0.8	>40
<b>5f</b>	>40	>40	>40	>40	>40	>40
<b>5g</b>	>40	29.9 ± 2.3	>40	30.7 ± 0.7	>40	>40
<b>5h</b>	>40	>40	>40	>40	>40	>40
<b>5i</b>	>40	>40	>40	>40	>40	>40
<b>7a</b>	>40	31.1 ± 0.8	13.1 ± 4.4	9.6 ± 0.2	18.4 ± 0.6	26.2 ± 4.3
<b>7b</b>	>40	39.8 ± 0.2	13.7 ± 0.8	15.4 ± 3.0	29.2 ± 1.7	37.2 ± 1.2
<b>7c</b>	>40	38.3 ± 0.0	15.6 ± 0.4	13.6 ± 1.1	36.8 ± 0.7	34.5 ± 2.2
<b>7d</b>	>40	35.0 ± 2.8	12.6 ± 2.3	9.4 ± 0.2	17.3 ± 0.1	37.5 ± 1.6
<b>8a</b>	>40	>40	6.2 ± 0.4	12.0 ± 1.0	14.2 ± 1.6	>40
<b>8b</b>	>40	>40	9.0 ± 0.2	13.7 ± 0.7	37.1 ± 0.9	>40
<b>8c</b>	>40	>40	8.2 ± 0.1	8.9 ± 0.4	33.8 ± 3.8	>40
<b>8d</b>	>40	>40	7.5 ± 0.3	7.4 ± 1.6	17.3 ± 3.2	>40
<b>SAHA</b>	0.02 ± 0.00	30.1 ± 4.9	12.4 ± 0.6	37.1 ± 1.3	37.7 ± 1.6	0.008 ± 0.001

<sup>a</sup>Each values are presented as the mean of three independent experiments.

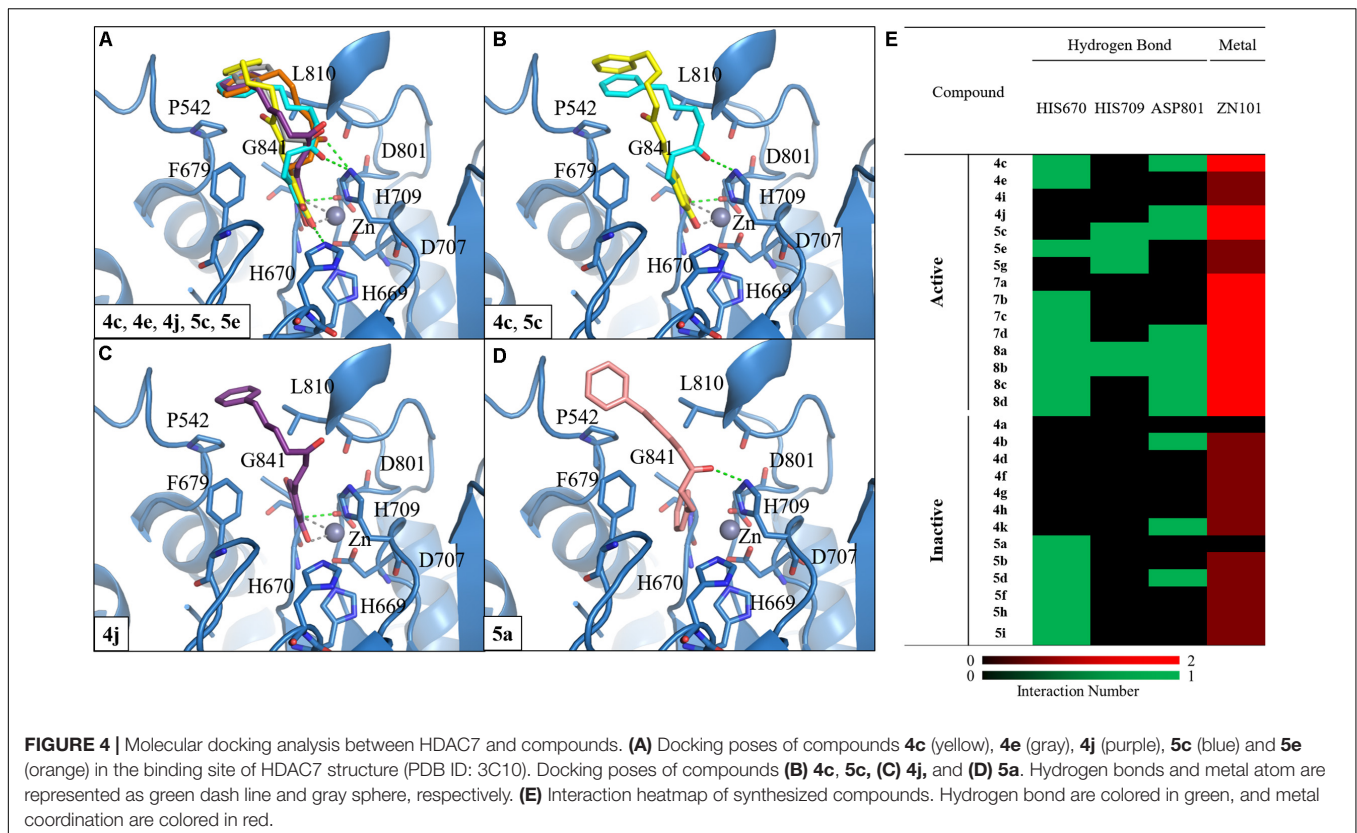
compound **5c** was the most potent, with IC<sub>50</sub> values of 18.1, 3.8, and 5.3 μM for HDAC4, 5, and 9, respectively. Compound **5c** showed enhanced inhibitory activity against class IIa HDACs compared to compound **4c**, suggesting that α, β-saturated compounds had slightly increased HDAC class IIa inhibitory activity compared to unsaturated compounds. Compound **4j** was the most potent HDAC7 inhibitor with an IC<sub>50</sub> value of 3.8 μM. The compounds that showed effective inhibitions of HDAC5 or HDAC7 contain a catechol or pyrogallol moiety as the A ring. This result demonstrated that catechol and pyrogallol moieties are an effective ZBG for class IIa HDACs.

Group two (compounds **7a–d** and **8a–d**) differ in the linker chain length. These compounds display selectivity toward class IIa HDAC (Table 2). The α, β-saturated groups on compounds **8a–d** slightly increase their potency of HDAC5 when compared to compounds **7a–d**. Nevertheless, the class IIa HDACs inhibitory activity of compounds **7a–d** and **8a–d** are inferior to that of compound **5c** (Table 2). In addition, compounds **7a–d** and **8a–d** show relatively poor inhibition toward HDAC7 when compared to compound **4j**. These results suggest that shortening the chain length and increasing the α,

β-unsaturation does not enhance the HDAC inhibitory activity in comparison with compound **5c**. Interestingly, the compounds **4c**, **4e**, **4j**, **5c**, **5e**, **7a–d**, and **8a–d** show effective Aβ<sub>1–42</sub> self-aggregation inhibition as described above.

### Molecular Docking Analysis of Compounds With HDAC7

We selected HDAC7 as the representative of class IIa HDACs to analyze compound interactions between our synthesized compounds. The compounds were docked into the binding site of HDAC7 (PDB ID: 3C10) with –CDOCKER Energy score ranged from 33 to 51. The RMSD analysis revealed that most binding poses are similar (Supplementary Figure S92). The total energy of protein-compound complexes can be found in Supplementary Table S2. The group one active compounds **4c**, **4e**, **4j**, **5c**, and **5e** contain a catechol or pyrogallol group as the ZBGs. The ZBG also facilitates hydrogen bonds for compounds **4c**, **4e**, **4j**, and **5c** and residue G841. In addition, all active compounds form a hydrogen bond with residue H670 (Figure 4A). Residue D801 also form hydrogen bonds with compounds **4c**, **4j**, and **5c**. The carbonyl, which is located on the linker, of compound **5c** has a



hydrogen bond interaction with residue H709. In addition, the benzene functions as the cap to create hydrophobic interactions with surface residues P542 or L810.

We observed different interactions between our synthesized active compounds and HDAC7. The active compounds **4c**, **4j**, and **5c** contain polar contacts to D801, G841 and hydrophobic contacts with P542 and L810. However, compound **5c** forms an extra hydrogen bond with residue H709. This increases the binding ability of compound **5c** (Figure 4B). In contrast, compound **4j** only forms hydrophobic interactions with residue H709 (Figure 4C). However, compound **4j** is a more potent inhibitor compared to compound **5c** (Table 2). The inactive compound **5a** ( $IC_{50} > 40 \mu M$ ) does not contain hydroxy groups on the A ring; therefore, it cannot coordinate with the zinc ion within the HDAC7 binding site (Figures 4D,E).

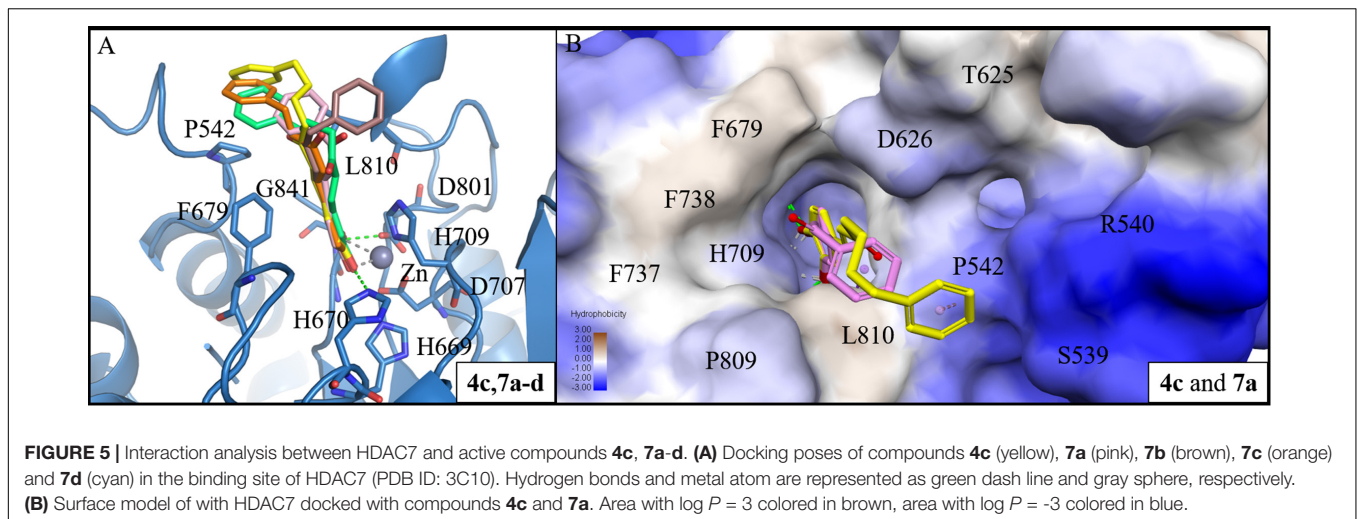
Next, we analyzed the interactions of group two active compounds **7a–d** and **8a–d**. We compared the docking poses of compounds **4c** and **7a–d** in HDAC7 (Figure 5A). Compound **4c** make hydrophobic contacts with cap residues P542, H709, and L810. In contrast, the shorter linker in compounds **7a–d** does not allow the benzene cap to sufficiently form interactions with cap residue L810. Compounds **7c** and **7d** contain a longer linker, two and three respectively, and were able to form a  $\pi$ -alkyl interaction with residue P542. Previous studies have suggested that the behavior of the cap group plays an important role in HDAC binding affinity (Wang et al., 2005). Thus, the shorter linker in our compounds reduces their ability to sufficiently interact with surface residues of HDAC7 (Figure 5B).

## Interaction Analysis of Compounds in $A\beta_{1-42}$ and HDAC7

We further analyzed common interactions of the compounds to elucidate their dual inhibitions against  $A\beta_{1-42}$  self-aggregation and HDAC7 (Figure 6). The interaction analysis of compound **5c** revealed structural features that contributes to the inhibition of  $A\beta_{1-42}$  self-aggregation and HDAC7. Compound **5c** contain features typical of HDAC inhibitors, which include a ZBG, a linker and a cap. The catechol moiety not only functions as the ZBG in HDAC7 but generates polar contacts with the electrically charged amino acid residue D23 in  $A\beta_{1-42}$ . The carbonyl group, located on the linker, generate polar contacts with residue H709 in HDAC7. The carbonyl moiety also creates a hydrogen bond with residue Q15 in  $A\beta_{1-42}$ . Almost all of the compounds synthesized in this study form hydrogen bonds with this residue in  $A\beta_{1-42}$ . Finally, the cap is a phenyl ring with a resonance system that created VDW interactions with residue V18 in  $A\beta_{1-42}$  and Pi-alkyl interactions with residues P542 and L810 HDAC7. The compounds synthesized in this study may provide an effective design for dual inhibitors of HDAC7 and  $A\beta_{1-42}$  self-aggregation.

## Cytotoxicity of Compounds **4j**, **5c**, **5e** and SAHA

Next, we evaluated the cytotoxicity of the identified compounds. Several studies indicate many methods can be used to evaluate the cytotoxicity, including primary neurons and neuroblastoma cells cultures (Shiple et al., 2016; Marangoni et al., 2018; Peng et al., 2018). Unfortunately, primary neuron cultures are



difficult to perform, since mature neurons do not undergo cell division. Previous researchers have used SH-SY5Y cells to test potential neurological drugs. For instance, *Achyranthes bidentata* polypeptides, a potential treatment for Parkinson's disease, shows 100% viability in SH-SY5Y cells, while rat primary dopaminergic neurons were found to be 95% viable (Peng et al., 2018). Treating SH-SY5Y cells with the neurotoxic agent 1-methyl-4-phenylpyridinium iodide at 100  $\mu\text{M}$  resulted in 80% cell viability, while primary rat mesencephalic neurons were reduced to roughly 75% viability (Luchtman et al., 2013). These results indicate that the cytotoxicity response of compounds in SH-SY5Y cells may be similar to primary cultured neurons. Due to the above reasons, we used SH-SY5Y cells to evaluate the cytotoxicity of our compounds.

Compounds **4j**, **5c**, and **5e** were the most potent inhibitors for HDAC5 or 7, and also showed  $\text{A}\beta_{1-42}$  self-aggregation inhibitory activity. The HDAC inhibitor SAHA was used as the reference to compare their cytotoxic effects. The cell viability was evaluated by 7-hydroxy-10-oxidophenoxazin-10-ium-3-one (resazurin, alamar blue) assay. As summarized in **Figure 7**, the three compounds did not show significant cytotoxicity at a high concentration (40  $\mu\text{M}$ ), which suggested that compounds **4j**, **5c**, and **5e** exhibited very low toxicity to SH-SY5Y cells compared to SAHA. In addition, the trypan blue exclusion test also shows the same trends (Supplementary Figure S93). Based on these results, compounds **4j**, **5c**, and **5e** were selected to test their neuroprotective effects.

### Neuroprotective Effect of Compounds **4j**, **5c**, and **5e** on $\text{H}_2\text{O}_2$ -Induced Cell Damage in SH-SY5Y Cells

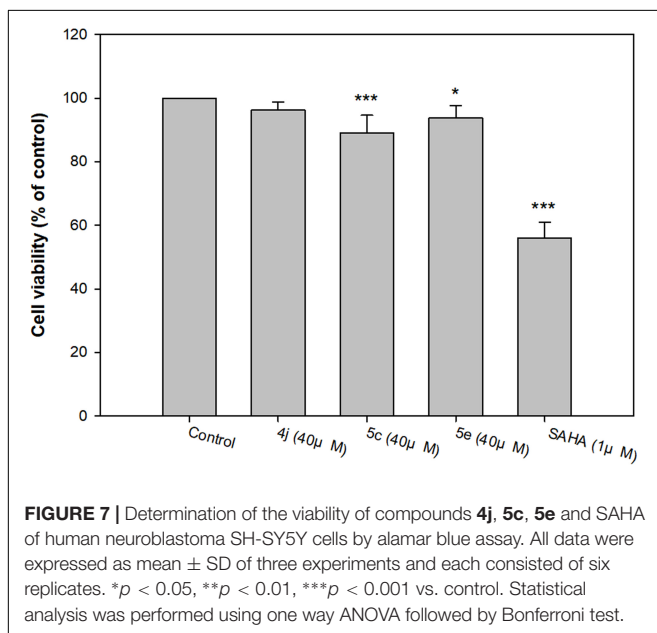
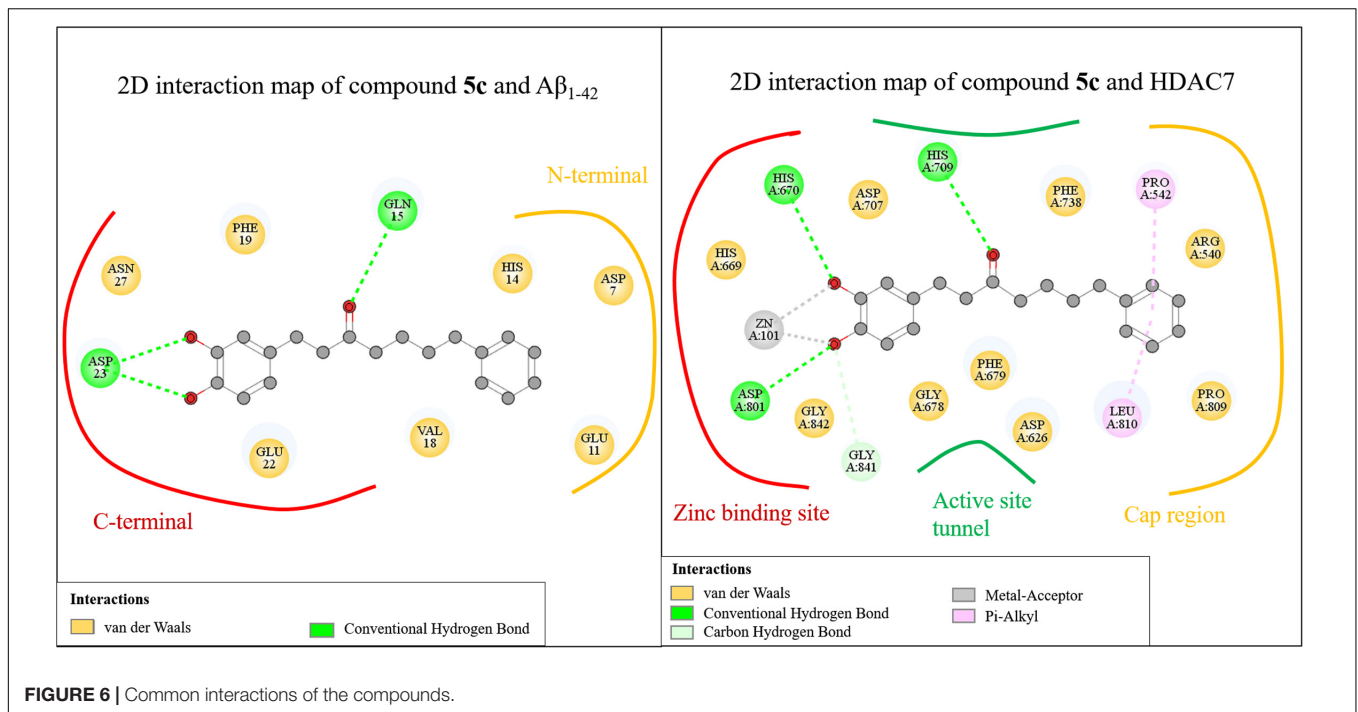
The neuroprotective capacities of compounds **4j**, **5c**, and **5e** against oxidative stress were evaluated at three different concentrations (40, 20, and 10  $\mu\text{M}$ ). After 500  $\mu\text{M}$   $\text{H}_2\text{O}_2$  exposure, cell viability was markedly decreased to 34.6%, suggesting a high sensitivity to  $\text{H}_2\text{O}_2$  induced SH-SY5Y cell injury (**Figure 8**). Compared to the untreated control, compounds **4j**, **5c**, and **5e** showed protective effects in a dose-dependent manner against  $\text{H}_2\text{O}_2$  induced SH-SY5Y cell

injury (**Figure 8**). At concentrations of 40  $\mu\text{M}$ , compounds **4j**, **5c**, and **5e** indicated significantly neuroprotective effects and the cell viabilities were 88.3, 61.3, and 58.8%, respectively. Moreover, the trypan blue exclusion test also shows the same trends (Supplementary Figure S94). Therefore, compounds **4j**, **5c**, and **5e** were able to protect these neurons from toxic stimuli induced by  $\text{H}_2\text{O}_2$ .

### Compounds **4j**, **5c**, and **5e** Have Potential Use as AD Therapeutics

Next, we looked to determine the compounds' ADMET properties (Supplementary Table S3). The BBB is one of the major impediments for neurological drugs. Compounds **5c** and **5e** was calculated to have a high BBB penetration, whereas compound **4j** had medium penetration. Furthermore, all three compounds showed good human intestinal absorption after oral administration. Finally, the aqueous solubility descriptor predicts the aqueous solubility of each compound in water at 25°C. The three compounds were predicted to be slightly soluble to soluble in water. Thus, compounds **4j**, **5c**, and **5e** are predicted to penetrate the BBB when administered orally.

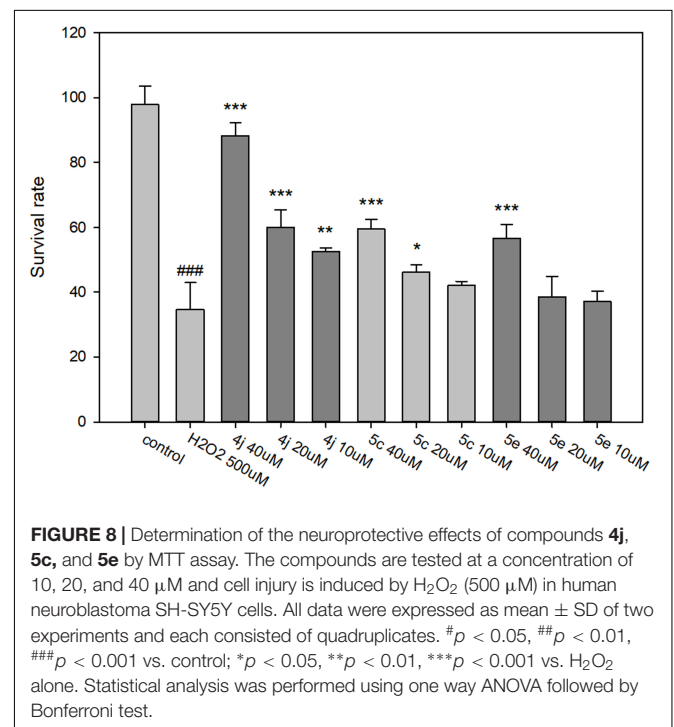
Alzheimer's disease is a complex disease with multiple pathogenic mechanisms.  $\text{A}\beta_{1-42}$  aggregation and HDAC overexpression have been shown to be involved in AD pathology. The  $\text{A}\beta_{1-42}$  isoform displays lower solubility and aggregation, which leads to toxic  $\text{A}\beta$  oligomers. Class IIa HDACs inhibitors affect the activities of the  $\beta$ -catenin (Margariti et al., 2010) and HSF1 (Calderwood and Murshid, 2017), which plays an important role in AD progression. Therefore, we developed dual inhibitors of  $\text{A}\beta_{1-42}$  self-aggregation and class IIa HDACs as potential AD treatment. A dual inhibitor has many advantages over a traditional single target inhibitor (Talevi, 2015). Single target drugs for AD treatment only offer a palliative treatment, whereas multi-target drugs have the potential to have an increased synergistic effect. A multi-target drug has a lower risk of drug-drug interactions compared to multicomponent drugs, or traditional drug cocktails (Morphy and Rankovic, 2005). Because of these reasons, we believe that compounds



**4j**, **5c**, and **5e** show great promise as AD therapeutics. Further studies will be needed to optimize their potency for use as AD treatment.

## CONCLUSION

Our study sought to develop novel inhibitors that can target both A $\beta$  and HDAC as a potential AD therapeutic. The A $\beta$  hypothesis is the most widely accepted for the



progression of AD. The self-aggregation of A $\beta$  leads to the formation of extracellular plaques and neurotoxicity. Additionally, class IIa HDACs are also implicated in AD development. For instance, overexpression of HDAC5 and HDAC7 is associated with various dysregulated biochemical pathways in AD. Due to this complexity,

a multi-target drug has great potential for better AD therapeutics. We designed and synthesized a series of diarylheptanoid derivatives with either a catechol or pyrogallol moiety, for A $\beta$  self-aggregation and HDAC inhibition. These moieties have been shown to inhibit A $\beta$  self-aggregation. Compounds **4j**, **5c**, and **5e** displayed potent inhibition of both A $\beta$ <sub>1–42</sub> self-aggregation and of class IIa isozymes HDAC5 and 7, with IC<sub>50</sub> values of <10  $\mu$ M. These active compounds contain three common features: (1) a catechol or pyrogallol moiety that not only creates hydrogen bonds with residue D23 of A $\beta$ , but also acts as a zinc binding group for HDAC inhibition, (2) a carbonyl that occupies the hydrophobic tunnel within the HDAC catalytic site that also creates a hydrogen bond with residue Q15 of A $\beta$ <sub>1–42</sub> structure, and (3) an aromatic ring that creates hydrophobic interactions with the N-terminal of A $\beta$ <sub>1–42</sub> but also functions as a cap for HDAC class IIa. In addition, compounds with shorter linkers were only able to inhibit A $\beta$ , but not HDAC7. In contrast, compounds with longer linkers, such as compounds **5j**, **5c**, and **5e**, showed favorable inhibitory activity for both A $\beta$  and HDAC7. The optimized linker for dual inhibitors were found to be a four carbon chain. Since our interest is in development of a dual inhibitor, these compounds were excluded from further study. Our *in vitro* studies showed no significant cytotoxicity toward SH-SY5Y cells when treated with compounds **4j**, **5c**, and **5e**, as well as a neuroprotective effect against H<sub>2</sub>O<sub>2</sub>-induced cell injury. In addition, the predicted BBB penetration, human intestinal absorption and aqueous solubility were favorable for compounds **4j**, **5c**, and **5e**. Taken together, these results reveal compounds **4j**, **5c**, and **5e** can act as a dual A $\beta$  self-aggregation and class IIa HDACs inhibitors. We believe that

these compounds can be used as lead compounds for AD drug development.

## AUTHOR CONTRIBUTIONS

L-CC, K-CH, and W-JH conceived and designed the experiments. L-CC, H-JT, C-YL, Y-YH, C-CY, and J-RW performed the experiments. L-CC, H-JT, C-YL, J-RW, Y-LL, W-CH, I-HP, K-KH, K-CH, and W-JH analyzed the data. L-CC, C-YL, TL, K-CH, and W-JH wrote the paper.

## FUNDING

We gratefully acknowledge the support from the Ministry of Science and Technology (MOST 106-2320-B-038-025 and MOST105-2320-B-038-024-MY3) and Program for Translational Innovation of Biopharmaceutical Development–Technology Supporting Platform Axis in Taiwan. This research was also partially supported by the Taiwan Protein Project (Grant No. 107-0210-01-19-02) and Health and welfare surcharge of tobacco products (Grant No. MOHW107-TDU-B-212-114020).

## SUPPLEMENTARY MATERIAL

The Supplementary Material for this article can be found online at: <https://www.frontiersin.org/articles/10.3389/fphar.2018.00708/full#supplementary-material>

## REFERENCES

- Ahn, H. J., Chen, Z. L., Zamolodchikov, D., Norris, E. H., and Strickland, S. (2017). Interactions of beta-amyloid peptide with fibrinogen and coagulation factor XII may contribute to Alzheimer's disease. *Curr. Opin. Hematol.* 24, 427–431. doi: 10.1097/MOH.0000000000000368
- Anderson, K. W., Chen, J., Wang, M., Mast, N., Pikuleva, I. A., and Turko, I. V. (2015). Quantification of histone deacetylase isoforms in human frontal cortex, human retina, and mouse brain. *PLoS One* 10:e0126592. doi: 10.1371/journal.pone.0126592
- BIOVIA, Dassault Systèmes (2016). *Discovery Studio Modeling Environment. Release 2017*. San Diego, CA: Dassault Systemes.
- Bolden, J. E., Peart, M. J., and Johnstone, R. W. (2006). Anticancer activities of histone deacetylase inhibitors. *Nat. Rev. Drug Discov.* 5, 769–784. doi: 10.1038/nrd2133
- Bu, X. L., Rao, P. P. N., and Wang, Y. J. (2016). Anti-amyloid aggregation activity of natural compounds: implications for Alzheimer's drug discovery. *Mol. Neurobiol.* 53, 3565–3575. doi: 10.1007/s12035-015-9301-4
- Calderwood, S. K., and Murshid, A. (2017). Molecular chaperone accumulation in cancer and decrease in Alzheimer's disease: the potential roles of HSF1. *Front. Neurosci.* 11:192. doi: 10.3389/fnins.2017.00192
- De Simone, A., Bartolini, M., Baschieri, A., Apperley, K. Y. P., Chen, H. H., Guardigni, M., et al. (2017). Hydroxy-substituted trans-cinnamoyl derivatives as multifunctional tools in the context of Alzheimer's disease. *Eur. J. Med. Chem.* 139, 378–389. doi: 10.1016/j.ejmech.2017.07.058
- Ding, F., Borreguero, J. M., Buldyrey, S. V., Stanley, H. E., and Dokholyan, N. V. (2003). Mechanism for the alpha-helix to beta-hairpin transition. *Proteins* 53, 220–228. doi: 10.1002/prot.10468
- Feng, C. W., Hung, H. C., Huang, S. Y., Chen, C. H., Chen, Y. R., Chen, C. Y., et al. (2016). Neuroprotective effect of the marine-derived compound 11-dehydrosinularioid through DJ-1-related pathway in *in vitro* and *in vivo* models of Parkinson's disease. *Mar. Drugs* 14:E187. doi: 10.3390/md14100187
- Fischer, A., Sananbenesi, F., Mungenast, A., and Tsai, L. H. (2010). Targeting the correct HDAC(s) to treat cognitive disorders. *Trends Pharmacol. Sci.* 31, 605–617. doi: 10.1016/j.tips.2010.09.003
- Gilbert, B. J. (2013). The role of amyloid beta in the pathogenesis of Alzheimer's disease. *J. Clin. Pathol.* 66, 362–366. doi: 10.1136/jclinpath-2013-201515
- Hardy, J., and Selkoe, D. J. (2002). The amyloid hypothesis of Alzheimer's disease: progress and problems on the road to therapeutics. *Science* 297, 353–356. doi: 10.1126/science.1072994
- Huang, W. J., Wang, Y. C., Chao, S. W., Yang, C. Y., Chen, L. C., Lin, M. H., et al. (2012). Synthesis and biological evaluation of ortho-aryl N-hydroxycinnamides as potent histone deacetylase (HDAC) 8 isoform-selective inhibitors. *ChemMedChem* 7, 1815–1824. doi: 10.1002/cmdc.20120300
- Hudson, S. A., Ecroyd, H., Kee, T. W., and Carver, J. A. (2009). The thioflavin T fluorescence assay for amyloid fibril detection can be biased by the presence of exogenous compounds. *FEBS J.* 276, 5960–5972. doi: 10.1111/j.1742-4658.2009.07307.x
- Hung, S. Y., and Fu, W. M. (2017). Drug candidates in clinical trials for Alzheimer's disease. *J. Biomed. Sci.* 24:47. doi: 10.1186/s12929-017-0355-7
- Jang, S., Jung, J. C., Kim, D. H., Ryu, J. H., Lee, Y., Jung, M., et al. (2009). The neuroprotective effects of benzylideneacetophenone derivatives on excitotoxicity and inflammation via phosphorylated Janus tyrosine kinase 2/phosphorylated signal transducer and activator of transcription 3 and mitogen-activated protein K pathways. *J. Pharmacol. Exp. Ther.* 328, 435–447. doi: 10.1124/jpet.108.144014
- Kerridge, C., Belyaev, N. D., Nalivaeva, N. N., and Turner, A. J. (2014). The Abeta-clearance protein transthyretin, like neprilysin, is epigenetically regulated by the

- amyloid precursor protein intracellular domain. *J. Neurochem.* 130, 419–431. doi: 10.1111/jnc.12680
- Koseki, T., Mouri, A., Mamiya, T., Aoyama, Y., Toriumi, K., Suzuki, S., et al. (2012). Exposure to enriched environments during adolescence prevents abnormal behaviours associated with histone deacetylation in phencyclidine-treated mice. *Int. J. Neuropsychopharmacol.* 15, 1489–1501. doi: 10.1017/S1461145711001672
- Kuperstein, I., Broersen, K., Benilova, I., Rozenski, J., Jonckheere, W., Debulpaep, M., et al. (2010). Neurotoxicity of Alzheimer's disease Abeta peptides is induced by small changes in the Abeta42 to Abeta40 ratio. *EMBO J.* 29, 3408–3420. doi: 10.1038/emboj.2010.211
- Lee, S. H., Lim, S. Y., Choi, J. H., Jung, J. C., Oh, S., Kook, K. H., et al. (2014). Benzylideneacetophenone derivatives attenuate IFN-gamma-induced IP-10/CXCL10 production in orbital fibroblasts of patients with thyroid-associated ophthalmopathy through STAT-1 inhibition. *Exp. Mol. Med.* 46:e100. doi: 10.1038/emm.2014.26
- Leon, R., Garcia, A. G., and Marco-Contelles, J. (2013). Recent advances in the multitarget-directed ligands approach for the treatment of Alzheimer's disease. *Med. Res. Rev.* 33, 139–189. doi: 10.1002/med.20248
- Luchtman, D. W., Meng, Q., Wang, X., Shao, D., and Song, C. (2013).  $\omega$ -3 fatty acid eicosapentaenoic acid attenuates MPP<sup>+</sup>-induced neurodegeneration in fully differentiated human SH-SY5Y and primary mesencephalic cells. *J. Neurochem.* 124, 855–868. doi: 10.1111/jnc.12068
- Marangoni, N., Kowal, K., Deliu, Z., Hensley, K., and Feinstein, D. L. (2018). Neuroprotective and neurotrophic effects of Lanthionine Ketimine Ester. *Neurosci. Lett.* 664, 28–33. doi: 10.1016/j.neulet.2017.11.018
- Margariti, A., Zampetaki, A., Xiao, Q., Zhou, B., Karamariti, E., Martin, D., et al. (2010). Histone deacetylase 7 controls endothelial cell growth through modulation of beta-catenin. *Circ. Res.* 106, 1202–1211. doi: 10.1161/CIRCRESAHA.109.213165
- Miller, T. A., Witter, D. J., and Belvedere, S. (2003). Histone deacetylase inhibitors. *J. Med. Chem.* 46, 5097–5116. doi: 10.1021/jm0303094
- Morphy, R., and Rankovic, Z. (2005). Designed multiple ligands. An emerging drug discovery paradigm. *J. Med. Chem.* 48, 6523–6543. doi: 10.1021/jm058225d
- Omar, S. H., Kerr, P. G., Scott, C. J., Hamlin, A. S., and Obied, H. K. (2017). Olive (*Olea europaea* L.) biophenols: a nutraceutical against oxidative stress in SH-SY5Y Cells. *Molecules* 22:E1858. doi: 10.3390/molecules2211858
- Peng, S., Wang, C., Ma, J., Jiang, K., Jiang, Y., Gu, X., et al. (2018). *Achyranthes bidentata* polypeptide protects dopaminergic neurons from apoptosis in Parkinson's disease models both in vitro and in vivo. *Br. J. Pharmacol.* 175, 631–643. doi: 10.1111/bph.14110
- Rafatian, G., Khodagholi, F., Farimani, M. M., Abraki, S. B., and Gardaneh, M. (2012). Increase of autophagy and attenuation of apoptosis by Salvigenin promote survival of SH-SY5Y cells following treatment with H<sub>2</sub>O<sub>2</sub>. *Mol. Cell. Biochem.* 371, 9–22. doi: 10.1007/s11010-012-1416-6
- Shipley, M. M., Mangold, C. A., and Szpara, M. L. (2016). Differentiation of the SH-SY5Y human neuroblastoma cell line. *J. Vis. Exp.* 108:53193. doi: 10.3791/53193
- Taguchi, R., Hatayama, K., Takahashi, T., Hayashi, T., Sato, Y., Sato, D., et al. (2017). Structure-activity relations of rosmarinic acid derivatives for the amyloid beta aggregation inhibition and antioxidant properties. *Eur. J. Med. Chem.* 138, 1066–1075. doi: 10.1016/j.ejmech.2017.07.026
- Talevi, A. (2015). Multi-target pharmacology: possibilities and limitations of the “skeleton key approach” from a medicinal chemist perspective. *Front. Pharmacol.* 6:205. doi: 10.3389/fphar.2015.00205
- Vallee, A., and Lecarpentier, Y. (2016). Alzheimer disease: crosstalk between the canonical Wnt/beta-catenin pathway and PPARs alpha and gamma. *Front. Neurosci.* 10:459. doi: 10.3389/fnins.2016.00459
- Volmar, C.-H., and Wahlestedt, C. (2015). Histone deacetylases (HDACs) and brain function. *Neuroepigenetics* 1, 20–27. doi: 10.1016/j.nepig.2014.10.002
- Wang, D. F., Helquist, P., Wiech, N. L., and Wiest, O. (2005). Toward selective histone deacetylase inhibitor design: homology modeling, docking studies, and molecular dynamics simulations of human class I histone deacetylases. *J. Med. Chem.* 48, 6936–6947. doi: 10.1021/jm0505011
- Wegener, D., Wirsching, F., Riestler, D., and Schwienhorst, A. (2003). A fluorogenic histone deacetylase assay well suited for high-throughput activity screening. *Chem. Biol.* 10, 61–68. doi: 10.1016/S1074-5521(02)00305-8
- Xu, Y. X., Wang, H., Li, X. K., Dong, S. N., Liu, W. W., Gong, Q., et al. (2018). Discovery of novel propargylamine-modified 4-aminoalkyl imidazole substituted pyrimidinylthiourea derivatives as multifunctional agents for the treatment of Alzheimer's disease. *Eur. J. Med. Chem.* 143, 33–47. doi: 10.1016/j.ejmech.2017.08.025
- Zhou, Y., Jiang, C., Zhang, Y., Liang, Z., Liu, W., Wang, L., et al. (2010). Structural optimization and biological evaluation of substituted bisphenol A derivatives as beta-amyloid peptide aggregation inhibitors. *J. Med. Chem.* 53, 5449–5466. doi: 10.1021/jm1000584

**Conflict of Interest Statement:** The authors declare that the research was conducted in the absence of any commercial or financial relationships that could be construed as a potential conflict of interest.

Copyright © 2018 Chen, Tseng, Liu, Huang, Yen, Weng, Lu, Hou, Lin, Pan, Huang, Huang and Hsu. This is an open-access article distributed under the terms of the Creative Commons Attribution License (CC BY). The use, distribution or reproduction in other forums is permitted, provided the original author(s) and the copyright owner(s) are credited and that the original publication in this journal is cited, in accordance with accepted academic practice. No use, distribution or reproduction is permitted which does not comply with these terms.